

MULTILEVEL MONTE CARLO METHODS FOR THE DEAN–KAWASAKI EQUATION FROM FLUCTUATING HYDRODYNAMICS

FEDERICO CORNALBA* AND JULIAN FISCHER†

ABSTRACT. Stochastic PDEs of Fluctuating Hydrodynamics are a powerful tool for the description of fluctuations in many-particle systems. In this paper, we develop and analyze a Multilevel Monte Carlo (MLMC) scheme for the Dean–Kawasaki equation, a pivotal representative of this class of SPDEs. We prove analytically and demonstrate numerically that our MLMC scheme provides a significant speed-up (with respect to a standard Monte Carlo method) in the simulation of the Dean–Kawasaki equation. Specifically, we quantify how the speed-up factor increases as the average particle density increases, and show that sizeable speed-ups can be obtained even in regimes of low particle density. Numerical simulations are provided in the two-dimensional case, confirming our theoretical predictions.

Our results are formulated entirely in terms of the law of distributions rather than in terms of strong spatial norms: this crucially allows for MLMC speed-ups altogether despite the Dean–Kawasaki equation being highly singular.

Key words. Multilevel Monte Carlo methods; Dean–Kawasaki equation; Fluctuating Hydrodynamics; Many-particle Systems.

1. INTRODUCTION

In the regime of large particle numbers, the behavior of interacting particle systems often gives rise to a classical PDE description, for instance in form of the classical equations of continuum mechanics. For medium-sized particle systems consisting of only, e.g., 10^5 – 10^9 particles, this idealized description often becomes insufficient, as thermal fluctuations may begin to impact the behavior. The theory of Fluctuating Hydrodynamics augments the classical PDEs of continuum mechanics with suitable noise terms to account for thermal fluctuations, giving rise to SPDE models; we refer the reader to Landau and Lifshitz [21], Spohn [24], and te Vrugt, Löwen and Wittkowski [25].

In this work, we are concerned with the numerical approximation of one of the most basic equations of Fluctuating Hydrodynamics, the *Dean–Kawasaki equation*

$$\partial_t \rho = \frac{1}{2} \Delta \rho + \nabla \cdot (\rho (\nabla V * \rho)) + N^{-1/2} \nabla \cdot (\sqrt{\rho} \xi). \quad (1.1)$$

It describes the effective behavior of the density ρ of a system of N weakly interacting diffusing particles $\{X_i(t)\}_{i=1}^N$ in the regime of large particle numbers $N \gg 1$. Here, V is

*UNIVERSITY OF BATH, CLAVERTON DOWN, BA2 7AY, BATH, UNITED KINGDOM

†INSTITUTE OF SCIENCE AND TECHNOLOGY AUSTRIA (ISTA), AM CAMPUS 1, 3400 KLOSTERNEUBURG, AUSTRIA.

E-mail addresses: fc402@bath.ac.uk, julian.fischer@ista.ac.at.

a (sufficiently regular) interaction potential and ξ denotes vector-valued space-time white noise. While the McKean-Vlasov equation $\partial_t \bar{\rho} = \frac{1}{2} \Delta \bar{\rho} + \nabla \cdot (\bar{\rho} (\nabla W * \bar{\rho}))$, obtained formally in the limit $N \rightarrow \infty$, describes the mean-field limit profile $\bar{\rho}$ of the particle system, the Dean-Kawasaki equation (1.1) for $N \gg 1$ in addition captures the law of the density fluctuations due to the finite number of particles.

The Dean-Kawasaki equation (1.1) is a highly singular SPDE; namely, it is even too singular to be renormalized by approaches like regularity structures or paracontrolled calculus [17, 16]. As shown in [19, 20], the only martingale solutions to (1.1) are in fact given by the empirical measures of the underlying particle system, that is $\rho(x, t) \equiv \mu_t^N(x) := N^{-1} \sum_{i=1}^N \delta(x - X_i(t))$. Nevertheless, a justification of SPDEs related to (1.1) has recently been given in [12, 10] in terms of large-deviation principles. Justifications for Dean-Kawasaki type models with regularized noise have been developed in [10, 11].

Recently, the authors and collaborators [7, 8] have shown that the Dean-Kawasaki equation may be viewed as a recipe for accurate and efficient simulations of the density fluctuations in the interacting particle system: When applying a formal spatial semi-discretization to (1.1), the law of density fluctuations predicted by the discretization accurately describes the law of density fluctuations in the underlying particle system, as long as the grid size satisfies $h \gg N^{-1/d}$ (d denotes the spatial dimension) – that is, as long as on average there is substantially more than one particle per grid cell.

Nevertheless, computing statistical properties of particle density fluctuations $\bar{\rho}$ such as variances $\mathbb{E}[|\int (\mu_t^N - \bar{\rho}^t)(x) \varphi(x) dx|^2]$ (for some test function φ) or higher moments such as $\mathbb{E}[|\int (\mu_t^N - \bar{\rho}^t)(x) \varphi(x) dx|^4]$ via discretizations of (1.1) is still a computationally demanding task, as in addition to solving an SPDE one needs to sample over many realizations of the noise. Multilevel Monte Carlo (MLMC) methods are a powerful numerical tool that often allows to offset a large amount of the sampling cost by performing the computation for most samples only on a much coarser numerical grid. Some of the first applications of MLMC methods have been in the context of statistical physics [3] and stochastic differential equations in mathematical finance [13]; they have since found widespread applications for random and stochastic PDEs, see for instance [2, 1, 4, 6, 9, 14, 15, 18].

In this work, we develop and analyze MLMC methods for the Dean-Kawasaki equation (1.1): In its strongest form, our main result informally reads:

Main Result (see Proposition 5.1 and Theorem 5.3 for precise details). *Let h_{\min} be a fixed grid size. Under suitable assumptions, and subject to the average particle density Nh_{\min}^d being large enough, we can set up a Multilevel Monte Carlo method for the simulation of (1.1) which has a speed-up factor $F \propto h_{\min}^{-(d \wedge 4)} \cdot |\log(h_{\min})|^{-1}$ with respect to the associated basic Monte Carlo method with the same grid size h_{\min} .*

For simplicity, we focus on the non-interacting case $V \equiv 0$ (in this case, $\bar{\rho}^t \equiv \mathbb{E}[\mu_t^N]$), although we expect that with the ideas of [8] one could generalize the result to interacting particles. Furthermore, we limit ourselves to the analysis of a finite difference scheme; due to the lack of regularity of solutions (see Figure 2 for a plot of a sample path), a finite element scheme would not offer compelling advantages.

As a key challenge for our analysis, unlike in Multilevel Monte Carlo approaches for parabolic SPDEs in the literature [2, 15], the highly singular nature of (1.1) equation prevents strong (pathwise) convergence of numerical solutions in the limit of arbitrarily

fine discretizations. Instead, convergence takes place only up to a minimal $h_{\min} \gg N^{-1/d}$, below which the sequence begins to diverge in C^0 . For an illustration of this lack of regularity and convergence of solutions, we refer to Figures 2–4 below. In addition, while microscopic fluctuations in (1.1) may be drastic, the macroscopic impact of fluctuations in (1.1) – i. e., the impact of fluctuations on weighted spatial averages like $\int \rho^t(x) \varphi(x) dx$ – is rather small due to the $N^{-1/2}$ prefactor of the noise. This discrepancy is directly related to the singular nature of the SPDE (1.1). It in particular forces us to work with stochastically weak convergence estimates – that is, convergence estimates for the law of distributions – to achieve an actual speed-up for computations. To the best of our knowledge, our present work is one of the first mathematical results on Multilevel Monte Carlo methods both for singular stochastic PDEs, and for stochastic PDEs involving multiplicative space-time white noise.

The paper is structured as follows. The basic notation is introduced in Section 2 (basic setup for discrete Dean–Kawasaki model) and Section 3 (Multi Level Monte Carlo setup). Assumptions, statements, and proofs of the main results are given in Sections 4, 5, and 6 respectively. Numerical results are discussed in Section 7.

2. BASIC NOTATION

We work with uniformly spaced grids on the spatial domain \mathbb{T}^d of the type $G_{h,d} := \{-\pi, -\pi + h, \dots, \pi - h\}^d$, for any compatible mesh-size $h > 0$. We denote by $(f_h, g_h)_h := h^d \sum_{x \in G_{h,d}} f_h(x) \cdot g_h(x)$ (respectively, $\|\cdot\|_h$) the inner product (respectively, the norm) on $L^2(G_{h,d})$. We denote by $\mathcal{I}_h: C(\mathbb{T}^d) \rightarrow L^2(G_{h,d})$ the pointwise interpolation operator. Furthermore, Δ_h, ∇_h denote discrete counterparts of Laplace and gradient operators (precise details are given later on). As for time, we work on a fixed interval $[0, T]$, and consider uniform partitions of the type $\mathcal{S}_\tau = \{0, \tau, \dots, T\}$, for a compatible time-step $\tau > 0$.

Definition 2.1 (Space-time discretised Dean–Kawasaki model). *We denote by $\rho_{h,\tau}$ the solution to the following finite-difference scheme for the Dean–Kawasaki dynamics associated with N independent Brownian motions in \mathbb{T}^d :*

$$\begin{aligned} \sum_{j=0}^1 a_j \rho_{h,\tau}^{m-j} &= \tau \sum_{j=0}^1 b_j \frac{1}{2} \Delta_h \rho_{h,\tau}^{m-j} \\ &+ N^{-1/2} \nabla_h \cdot \left(\sum_{(y,r) \in (G_{h,d}, \{1, \dots, d\})} \sqrt{[\rho_{h,\tau}^{m-1}]^+} e_{h,y,r}^d \right) \Delta \beta_{(y,r)}^{m-1}, \end{aligned} \quad (2.1)$$

started from $\rho_{h,\tau}^0 = \rho_{0,h}$, and where

- $\Delta \beta_{(y,r)}^{m-1} := \beta_{(y,r)}(m\tau) - \beta_{(y,r)}((m-1)\tau)$ are increments for a family of independent Brownian motions $\{\beta_{(y,r)}\}_{(y,r) \in (G_{h,d}, \{1, \dots, d\})}$;
- $\rho_{h,0}$ is a suitable – possibly random – initial profile;
- $\{e_{h,y,r}^d\}_{(y,r) \in (G_{h,d}, \{1, \dots, d\})}$ is the orthonormal basis of $[L^2(G_{h,d})]^d$ given by $e_{h,y,r}^d(z) := h^{-d/2} \delta_{y \equiv z} f_r$, where $\{f_r\}_{r=1}^d$ is the canonical basis of \mathbb{R}^d ;
- $\{a_j\}_{j=0}^1, \{b_j\}_{j=0}^1$ are fixed weights determining the specific nature of the (one-step) time discretisation scheme.

3. MLMC FRAMEWORK

The goal is to compute statistical properties of the particle density fluctuations. Specifically, we aim to compute the expected value of random variables of the form

$$Q := \psi \left(N^{1/2} \int (\mu_N^T - \bar{\rho}^T)(x) \varphi(x) dx \right) \quad (3.1)$$

for sufficiently regular test functions ψ, φ . In order to approximate $\mathbb{E}[Q]$, we can compute the expected value of the quantity

$$P := \psi \left(N^{1/2} (\rho_{h,\tau}^T - \mathbb{E}[\rho_{h,\tau}^T], \mathcal{I}_h \varphi)_h \right), \quad (3.2)$$

where $\rho_{h,\tau}$ is the solution to the discrete Dean–Kawasaki model (2.1) with space (respectively, time) discretisation parameter h (respectively, τ). We think of the parameters (h, τ) in the random variable P introduced in (3.2) as being the smallest in a sequence of space/time parameters (so, effectively, $h \equiv h_{\min}, \tau = \tau_{\min}$): therefore, we construct a MLMC scheme for approximating $\mathbb{E}[P]$ by using the auxiliary quantities

$$P_\ell := \psi \left(N^{1/2} (\rho_{h_\ell, \tau_\ell}^T - \bar{\rho}_{h_\ell, \tau_\ell}^T, \mathcal{I}_{h_\ell} \varphi)_{h_\ell} \right), \quad (3.3)$$

on levels $\ell = \ell_0, \dots, L$, where

$$(h_\ell, \tau_\ell) := (h_{\min} \cdot \kappa_x^{L-\ell}, \tau_{\min} \cdot \kappa_t^{L-\ell}), \quad \ell = \ell_0, \dots, L, \quad (3.4)$$

for some $\kappa_x, \kappa_t \in \mathbb{N}$ to be specified. With this notation, $P_L \equiv P$, $(h_{\min}, \tau_{\min}) \equiv (h_L, \tau_L)$, and $(h_{\max}, \tau_{\max}) \equiv (h_{\ell_0}, \tau_{\ell_0})$. We use μ to denote the CFL ratio $\mu := \tau/h^2$ (obvious extensions for subscripts ℓ, \min, \max). When there is no ambiguity, we may choose to simplify the notation related to the level ℓ : for instance, we abbreviate $\psi(N^{1/2}(\rho_\ell^T - \bar{\rho}_\ell^T, \varphi_\ell)_\ell) \equiv \psi(N^{1/2}(\rho_{h_\ell, \tau_\ell}^T - \bar{\rho}_{h_\ell, \tau_\ell}^T, \mathcal{I}_{h_\ell} \varphi)_{h_\ell})$.

We consider two alternative ways to couple the noise on consecutive levels $\ell - 1, \ell$.

3.1. First coupling: Fourier frequencies. We split the spatial grid in three at each level increment (i.e., $\kappa_x = 3$ in (3.4)). We write the stochastic noise of (2.1) using a Fourier expansion in space, and standard coupling in time. In words, at the coarse level $\ell - 1$:

- all Fourier frequencies coming from the finer level ℓ are reused, and
- noise increments are obtained by summing up noise increments at level ℓ .

Explicitly, denoting the set of frequencies $I_\ell := \{-\pi h_\ell^{-1}; -\pi h_\ell^{-1} + 1; \dots; \pi h_\ell^{-1} - 1\}^d$, the noise increments at levels $\ell - 1$ and ℓ are given by

$$\begin{aligned} & W_\ell(x, t + \tau_\ell) - W_\ell(x, t) \\ &:= \sum_{(\xi, r) \in (I_\ell, \{1, \dots, d\})} e^{ix \cdot \xi} f_r(\beta_{\xi, r}(t + \tau_\ell) - \beta_{\xi, r}(t)), \quad \text{for } (x, t) \in G_{\ell, d} \times \mathcal{S}_\ell, \\ & W_{\ell-1}(x, t + \tau_{\ell-1}) - W_{\ell-1}(x, t) \\ &:= \sum_{j=0}^{\kappa_t-1} \sum_{(\xi, r) \in (I_{\ell-1}, \{1, \dots, d\})} e^{ix \cdot \xi} f_r[\beta_{\xi, r}(t + (j+1)\tau_\ell) - \beta_{\xi, r}(t + j\tau_\ell)], \\ & \quad \text{for } (x, t) \in G_{\ell-1, d} \times \mathcal{S}_{\ell-1}, \end{aligned}$$

where $\{\beta_{\xi, r}\}_{(\xi, r) \in (I_{\ell-1}, \{1, \dots, d\})}$ are standard independent Brownian motions.

3.2. Second coupling: Right-Most neighbourhood. While the coupling in time is the same as in the previous case, coupling in space is obtained by summing up noise increments in a “Right-Most” neighbourhood of each spatial point. Specifically, splitting the spatial grid in two at each level increment (i.e., $\kappa_x = 2$ in (3.4)), if we set $B_{\ell-1}^{\rightarrow}(x) := \{x + h_{\ell}v : v \in \{0; 1\}^d\}$ for each $x \in G_{\ell-1,d}$, we define

$$\begin{aligned} & W_{\ell}(x, t + \tau_{\ell}) - W_{\ell}(x, t) \\ & := \sum_{(y,r) \in (G_{\ell-1,d}, \{1, \dots, d\})} e_{h_{\ell}, y, r}^d(x) (\beta_{y,r}(t + \tau_{\ell}) - \beta_{y,r}(t)), \quad \text{for } (x, t) \in G_{\ell,d} \times \mathcal{S}_{\ell}, \\ & W_{\ell-1}(x, t + \tau_{\ell-1}) - W_{\ell-1}(x, t) \\ & := \sum_{(y,r) \in (G_{\ell-1,d}, \{1, \dots, d\})} e_{h_{\ell-1}, y, r}^d(x) \sum_{j=0}^{\kappa_t-1} (\tilde{\beta}_{y,r}(t + (j+1)\tau_{\ell}) - \tilde{\beta}_{y,r}(t + j\tau_{\ell})), \\ & \quad \text{for } (x, t) \in G_{\ell-1,d} \times \mathcal{S}_{\ell-1}, \end{aligned}$$

where $\tilde{\beta}_{y,r} := 2^{-d/2} \sum_{z \in B_{\ell-1}^{\rightarrow}(y)} \beta_{z,r}$, with $\{\beta_{\ell, z, r}\}_{(z,r) \in (G_{\ell-1,d}, \{1, \dots, d\})}$ being standard independent Brownian motions.

4. ASSUMPTIONS

We work under the following assumptions.

Assumption A1 (Parameter scaling). We choose N to be sufficiently large so that the following scaling

$$Nh_{\ell}^d \geq Kh_{\ell}^{-\alpha} (1 \vee \mu_{\ell}^2) |\log h_{\ell}|, \quad \ell \in \{\ell_0 + 1, \dots, L\}, \quad (4.1)$$

where $\mu_{\ell} := \tau_{\ell}/h_{\ell}^2$, holds for some fixed $\alpha > 0$ and some fixed $K > 0$.

Assumption A2 (Discrete Dean–Kawasaki dynamics). With regards to (2.1): i) we fix $a_0 = 1, a_1 = -1$; ii) the operators Δ_h and ∇_h are second-order finite difference operators in the spatial discretisation; iii) the couples $\{h_{\ell}, \tau_{\ell}\}_{\ell}$ are such that the noise-less version of the scheme (2.1) is stable for all ℓ .

Assumption A3 (Continuous Mean Field Limit). We assume the continuous mean field limit $\bar{\rho}^t$ to be strictly positive and bounded ($0 < \rho_{\min} \leq \bar{\rho}^t(x) \leq \rho_{\max}$), and satisfying $\bar{\rho}^t \in C^{R+3}$ for some $R > 4 + d/2$ in the case of Fourier coupling (Subsection 3.1), or $\bar{\rho}^t \in C^2$ in the case of Right-Most neighbour coupling (Subsection 3.2).

Assumption A4 (Test functions). For ψ, φ introduced in (3.2), we require that

$$\sup_{z \in \mathbb{R}^K} |\nabla \psi(z)| / (1 + |z|^r) \leq C, \quad \text{for some } r > 0, \quad (4.2)$$

and that $\varphi \in C^{R+4}$ for some $R > 4 + d/2$ in the case of Fourier coupling (Subsection 3.1), or $\varphi \in C^3$ in the case of Right-Most neighbour coupling (Subsection 3.2). Furthermore, we use the notation ϕ^t (respectively, ϕ_{ℓ}^t) to indicate the solution to the continuous (respectively, discrete) backwards heat equation ending at $\phi^T = \varphi$ (respectively, at $\phi_{\ell}^T = \mathcal{I}_{\ell}\varphi$).

Assumption A5 (Initial datum). We set the initial condition of the discrete mean field limit $\bar{\rho}_\ell^0 := \mathcal{I}_{h_\ell} \bar{\rho}^0$. We require the following bound for large fluctuations

$$\mathbb{E}[\|\rho_\ell^0 - \bar{\rho}_\ell^0\|_\infty^j] \lesssim j^j \left(N^{-1/2} h_\ell^{-d/2} \right)^j, \quad j \in \mathbb{N}, \quad (4.3)$$

see for instance [5, Theorem 3.4–3.5] and [22], as well as the fluctuation bound

$$\mathbb{E} \left[\left| N^{1/2} (\rho_\ell^0 - \bar{\rho}_\ell^0, \phi_\ell^0)_\ell - N^{1/2} \int (\mu_0^N - \bar{\rho}^0)(x) \phi^0(x) dx \right|^4 \right]^{1/4} \lesssim C(\varphi) h_\ell^2, \quad (4.4)$$

see also [8, Bound (3.10)].

Remark 4.1. The scaling (4.1) imposes that the average particle density per grid cell (i.e., Nh_ℓ^d) exceed a given threshold. The role of the terms $h_\ell^{-\alpha}$ and $(1 \vee \mu_\ell^2)$ will become apparent in due course. Assumption A5 is related to a fairly standard concentration inequality, see also similar discussions in [7, 8].

5. MAIN RESULTS

The main result of this paper (Theorem 5.3 below) directly stems from the following Proposition.

Proposition 5.1 (Bounding $\text{Var} \{P_\ell - P_{\ell-1}\}$). *Assume the validity of Assumptions A1, A2, A3, A4, A5, and set $\mu_\ell := \tau_\ell/h_\ell^2$. We have the estimate*

$$\begin{aligned} \text{Var}[P_\ell - P_{\ell-1}] & \lesssim_\varphi \min \left\{ \exp \left(- \frac{C \rho_{\min}}{\rho_{\max}^{1/2}} \left[\frac{N h_\ell^d}{\mu_\ell^2 \vee 1} \right]^{\frac{1}{2}} \right) \left[N^{-1} h_\ell^{-d} (\mu_\ell^2 \vee 1) \right]^{\frac{1}{2}} + \rho_{\min}^{-1} \left[N^{-1} h_\ell^{-d} (\mu_\ell^2 \vee 1) \right]; \right. \\ & \left. \left[N^{-1} h_\ell^{-d} (\mu_\ell^2 \vee 1) \right]^{\frac{1}{2}} \right\} + \text{Err}_{num} := \text{Err}_{mod} + \text{Err}_{num}, \end{aligned} \quad (5.1)$$

where

$$\text{Err}_{num} = \begin{cases} \min[\rho_{\min}^{-1}(h_\ell^4 + \tau_\ell^2), h_\ell^2 + \tau_\ell] + C(\rho_{\min})[h_\ell^4 + \tau_\ell^2], & \text{for Fourier coupling,} \\ \min\{\rho_{\min}^{-1}(h_\ell^2 + \tau_\ell), h_\ell + \tau_\ell\}, & \text{for R-M coupling.} \end{cases}$$

Remark 5.2. Bound (5.1) in Proposition 5.1 may take several forms, depending on the choice of coupling, on which of the arguments in the minima is smaller, and on whether or not Err_{mod} is dominated by Err_{num} . As we do not want to unnecessarily overcomplicate the statement of our main Theorem 5.3 (which stems directly from Proposition 5.1), we limit ourselves to stating Theorem 5.3 in two relevant subset of cases, one for each coupling.

Theorem 5.3 (Speed-up for MLMC estimator). *Assume the validity of Assumptions A1, A2, A3, A4, A5. Let M_ℓ , $\ell \in \{\ell_0 + 1, \dots, L\}$ be the number of samples of $P_\ell - P_{\ell-1}$, and let M_{ℓ_0} be the number of samples of P_{ℓ_0} . Set*

$$M_l := \lceil h_\ell/h_{\min} \rceil^d \cdot \lceil \tau_\ell/\tau_{\min} \rceil \quad (5.2)$$

and ℓ_0 such that $L - \ell_0 \propto (\alpha \wedge d) |\log(h_{\min})|$ (α is introduced in Assumption A1). Assume the constant K in Assumption A1 to be large enough. Assume $\bar{\rho}$ to be regular enough so

that the order in the h -bound for Err_{num} in (5.1) is the highest of the two available (i.e., 4 for Fourier coupling, 2 for Right-Most coupling).

Then the variance of the Multilevel Monte Carlo estimator

$$\mu_{MLMC} := M_{\ell_0}^{-1} \sum_{i=1}^{M_{\ell_0}} P_{\ell_0,(i)} + \sum_{\ell=\ell_0+1}^L M_{\ell}^{-1} \sum_{i=1}^{M_{\ell}} (P_{\ell,(i)} - P_{\ell-1,(i)}) \quad (5.3)$$

satisfies the bound

$$Var[\mu_{MLMC}] \lesssim \begin{cases} h_{\min}^{\alpha \wedge d \wedge 4} & \text{for Fourier coupling} \\ h_{\min}^{\alpha \wedge d \wedge 2} & \text{for Right-Most coupling} \end{cases} \quad (5.4)$$

– where α is introduced in Assumption A1 – while carrying a total computational cost

$$Cost_{tot}(\mu_{MLMC}) \propto h_{\min}^{-d} \cdot \tau_{\min}^{-1} \cdot |\log(h_{\min})|. \quad (5.5)$$

As a result of (5.4)–(5.5), and of systematic error estimates from [7, Theorem 2], we deduce that using the MLMC estimator μ_{MLMC} defined in (5.3) to approximate

$$\mathbb{E} \left[\psi \left(N^{1/2} \int (\mu_N^T - \bar{\rho}^T)(x) \varphi(x) dx \right) \right]$$

(see (3.1)) – as opposed to a standard MC estimator on the finest scale (h_{\min}, τ_{\min}) – grants a computational speed-up factor

$$F \propto \begin{cases} h_{\min}^{-(\alpha \wedge d \wedge 4)} \cdot |\log(h_{\min})|^{-1} & \text{for Fourier coupling,} \\ h_{\min}^{-(\alpha \wedge d \wedge 2)} \cdot |\log(h_{\min})|^{-1} & \text{for Right-Most coupling.} \end{cases} \quad (5.6)$$

Remark 5.4. Theorem 5.3 essentially says that, when using Right-Most coupling, the gain factor of MLMC over standard MC is proportional to $h_{\min}^{-(\alpha \wedge d)}$ (up to logarithmic factor) in dimension $d \leq 2$, provided the average particle density per grid cell Nh_{\min}^d be large enough. The Fourier coupling extends the estimate also to $d \in \{3; 4\}$.

6. PROOFS OF PROPOSITION 5.1 AND THEOREM 5.3

The following Lemma – whose proof is deferred to Appendix B – is needed for proving Proposition 5.1.

Lemma 6.1. Under Assumption A5 and Assumption A1 (with $\alpha = 0$) we have

$$\mathbb{P} \left[\sup_{t \in \mathcal{S}_\tau} \|\rho_{h,\tau}^t - \bar{\rho}_{h,\tau}^t\|_\infty \geq \frac{B\rho_{\min}}{4} \right] \lesssim \exp \left(-\frac{C\rho_{\min}}{\rho_{\max}^{1/2}} \left[\frac{Nh^d}{\mu^2 \vee 1} \right]^{1/2} \frac{B}{\sqrt{B+1}} \right) \quad (6.1)$$

for any $B \geq 0$, and where $\mu = \tau/h^2$. Furthermore, we have the estimates

$$\mathbb{E} \left[\sup_{t \in \mathcal{S}_\tau} \|\rho_{h,\tau}^t - \bar{\rho}_{h,\tau}^t\|_\infty^j \right]^{1/j} \lesssim C(j) \rho_{\max}^{1/2} (N^{-1}h^{-d})^{1/2} (\mu^2 \vee 1)^{1/2}, \quad (6.2)$$

$$\mathbb{E} \left[|(\rho_{h,\tau}^t - \bar{\rho}_{h,\tau}^t, \mathcal{I}_h \varphi)_\ell|^j \right]^{1/j} \lesssim C(j) \rho_{\max}^{1/2} N^{-1/2} \|\varphi\|_{C^1}. \quad (6.3)$$

6.1. Proof of Proposition 5.1 with Fourier coupling. For notational convenience, we occasionally drop the time dependence, and the vectorial notation over the d components of the noise (i.e., we write $e^{ix \cdot \xi}$ in spite of $\{e^{ix \cdot \xi} f_r\}_{r=1}^d$).

Step 1: rewriting $\text{Var}[P_\ell - P_{\ell-1}]$. A first-order Taylor expansion on ψ gives

$$\begin{aligned} & \text{Var}[P_\ell - P_{\ell-1}] \\ & \leq \mathbb{E}[|P_\ell - P_{\ell-1}|^2] \\ & = \mathbb{E}\left[\left|\psi(N^{1/2}(\rho_\ell^T - \bar{\rho}_\ell^T, \varphi_\ell)_\ell) - \psi(N^{1/2}(\rho_{\ell-1}^T - \bar{\rho}_{\ell-1}^T, \varphi_{\ell-1})_{\ell-1})\right|^2\right] \\ & \leq \mathbb{E}[|\nabla\psi(z)|^4]^{\frac{1}{2}} \mathbb{E}\left[\left|N^{\frac{1}{2}}[(\rho_\ell^T - \bar{\rho}_\ell^T, \varphi_\ell)_\ell - (\rho_{\ell-1}^T - \bar{\rho}_{\ell-1}^T, \varphi_{\ell-1})_{\ell-1}]\right|^4\right]^{\frac{1}{2}} \end{aligned} \quad (6.4)$$

for some random z such that

$$|z| \leq \max\left\{|N^{1/2}(\rho_\ell^T - \bar{\rho}_\ell^T, \varphi_\ell)_\ell|; |N^{1/2}(\rho_{\ell-1}^T - \bar{\rho}_{\ell-1}^T, \varphi_{\ell-1})_{\ell-1}|\right\}. \quad (6.5)$$

Step 2: bounding $\mathbb{E}[|\nabla\psi(z)|^4]$ in (6.4). Using (4.2), (6.5) and (6.3), we get

$$\mathbb{E}[|\nabla\psi(z)|^4] \leq C(\rho_{\max}, j) \|\varphi\|_{C^1}^{4r}. \quad (6.6)$$

Step 3: Itô formula for second term in right-hand-side of (6.4). Let the test functions ϕ_ℓ (respectively, $\phi_{\ell-1}$) satisfy the backwards evolution (A.1) ending in φ_ℓ (respectively, in $\varphi_{\ell-1}$). Thanks to the discrete martingale property in Lemma A.4 and a simple interpolation argument on the noise, we can define a continuous-time martingale $D_{\ell, \ell-1}^t$ such that, crucially,

$$D_{\ell, \ell-1}^t = N^{1/2}(\rho_\ell^t - \bar{\rho}_\ell^t, \phi_\ell^t)_\ell - N^{1/2}(\rho_{\ell-1}^t - \bar{\rho}_{\ell-1}^t, \phi_{\ell-1}^t)_{\ell-1} \quad \text{for all } t \in \mathcal{S}_{\ell-1}.$$

Now abbreviate $t_{\leftarrow}^\ell := \max\{m \in \mathcal{S}_{\tau_\ell} : m < t\}$. Using the continuous Itô Lemma, the noise coupling as stated in Subsection 3.1, and the error bound (A.4), we deduce

$$\begin{aligned} & \mathbb{E}[(D_{\ell, \ell-1}^z)^4] \\ & \lesssim \mathbb{E}[(D_{\ell, \ell-1}^0)^4] \\ & \quad + \int_0^z \mathbb{E}\left[(D_{\ell, \ell-1}^t)^2 \times \tau_\ell^2 + (D_{\ell, \ell-1}^t)^2 \times \right. \\ & \quad \times \left. \left\{ \sum_{\xi \in I_{\ell-1}} \left| \left(\sqrt{\rho_\ell^{t_{\leftarrow}^\ell, +}} e^{i\xi(\cdot)}, \nabla_\ell \phi_\ell^{t_{\leftarrow}^\ell} \right)_\ell - \left(\sqrt{\rho_{\ell-1}^{t_{\leftarrow}^{\ell-1}, +}} e^{i\xi(\cdot)}, \nabla_{\ell-1} \phi_{\ell-1}^{t_{\leftarrow}^{\ell-1}} \right)_{\ell-1} \right|^2 \right. \right. \\ & \quad \left. \left. + \sum_{\xi \in I_\ell \setminus I_{\ell-1}} \left| \left(\sqrt{\rho_\ell^{t_{\leftarrow}^\ell, +}} e^{i\xi(\cdot)}, \nabla_\ell \phi_\ell^{t_{\leftarrow}^\ell} \right)_\ell \right|^2 \right\} \right] dt \\ & =: \mathbb{E}[(D_{\ell, \ell-1}^0)^4] + \tau_\ell^4 + \int_0^z \mathbb{E}[(D_{\ell, \ell-1}^t)^2 \times \{A_{I_{\ell-1}} + A_{I_\ell \setminus I_{\ell-1}}\}] dt, \end{aligned} \quad (6.7)$$

where (\cdot) in $e^{i\xi(\cdot)}$ is reserved for the spatial variable x . The inequality (6.7) implies

$$\begin{aligned} & \mathbb{E}[(D_{\ell, \ell-1}^z)^4] \\ & \lesssim \mathbb{E}[(D_{\ell, \ell-1}^0)^4] + \tau_\ell^4 + \int_0^z \mathbb{E}[(D_{\ell, \ell-1}^t)^4] dt + \int_0^z \mathbb{E}[A_{I_{\ell-1}}^2 + A_{I_\ell \setminus I_{\ell-1}}^2] dt. \end{aligned} \quad (6.8)$$

Step 4: bounding $A_{I_{\ell-1}}^2$ in (6.8). By adding and subtracting zero we get

$$\begin{aligned}
A_{I_{\ell-1}} &\lesssim \sum_{\xi \in I_{\ell-1}} \left| \left(\sqrt{\rho_{\ell}^{t_{\leftarrow}^{\ell,+}}} e^{i\xi(\cdot)}, \nabla_{\ell} \phi_{\ell}^{t_{\leftarrow}^{\ell}} \right)_{\ell} - \left(\sqrt{\bar{\rho}^{t_{\leftarrow}^{\ell}}} e^{i\xi(\cdot)}, \nabla \phi_{\ell}^{t_{\leftarrow}^{\ell}} \right)_{\ell} \right|^2 \\
&\quad + \sum_{\xi \in I_{\ell}} \left| \left(\sqrt{\bar{\rho}^{t_{\leftarrow}^{\ell}}} e^{i\xi(\cdot)}, \nabla \phi_{\ell}^{t_{\leftarrow}^{\ell}} \right)_{\ell} - \left(\sqrt{\bar{\rho}^{t_{\leftarrow}^{\ell-1}}} e^{i\xi(\cdot)}, \nabla \phi_{\ell}^{t_{\leftarrow}^{\ell-1}} \right)_{\ell} \right|^2 \\
&\quad + \sum_{\xi \in I_{\ell-1}} \left| \left(\sqrt{\bar{\rho}^{t_{\leftarrow}^{\ell-1}}} e^{i\xi(\cdot)}, \nabla \phi_{\ell}^{t_{\leftarrow}^{\ell-1}} \right)_{\ell} - \left(\sqrt{\bar{\rho}^{t_{\leftarrow}^{\ell-1}}} e^{i\xi(\cdot)}, \nabla \phi_{\ell}^{t_{\leftarrow}^{\ell-1}} \right)_{\ell-1} \right|^2 \\
&\quad + \sum_{\xi \in I_{\ell-1}} \left| \left(\sqrt{\rho_{\ell-1}^{t_{\leftarrow}^{\ell-1,+}}} e^{i\xi(\cdot)}, \nabla_{\ell-1} \phi_{\ell-1}^{t_{\leftarrow}^{\ell-1}} \right)_{\ell-1} - \left(\sqrt{\bar{\rho}^{t_{\leftarrow}^{\ell-1}}} e^{i\xi(\cdot)}, \nabla \phi_{\ell}^{t_{\leftarrow}^{\ell-1}} \right)_{\ell-1} \right|^2 \\
&=: R_{\ell} + R_{t_{\leftarrow}^{\ell}, t_{\leftarrow}^{\ell-1}} + R_{\ell, \ell-1} + R_{\ell-1}.
\end{aligned} \tag{6.9}$$

Adding and subtracting zero (and dropping the dependence on t_{\leftarrow}^{ℓ}), we obtain

$$\begin{aligned}
R_{\ell} &\lesssim \sum_{\xi \in I_{\ell-1}} \left| \left(\left[\sqrt{\rho_{\ell}^+} - \sqrt{\bar{\rho}} \right] e^{i\xi(\cdot)}, \nabla_{\ell} \phi_{\ell} \right)_{\ell} - \left(\sqrt{\bar{\rho}} e^{i\xi(\cdot)}, [\nabla \phi - \nabla_{\ell} \phi_{\ell}] \right)_{\ell} \right|^2 \\
&\lesssim \left\| \left[\sqrt{\rho_{\ell}^+} - \sqrt{\bar{\rho}} \right] \nabla_{\ell} \phi_{\ell} \right\|_{\ell}^2 + \left\| \sqrt{\bar{\rho}} [\nabla \phi - \nabla_{\ell} \phi_{\ell}] \right\|_{\ell}^2 \\
&\lesssim \mathbf{1}_{\inf \rho_{\ell} \leq K} \left\| \left[\sqrt{\rho_{\ell}^+} - \sqrt{\bar{\rho}} \right] \nabla_{\ell} \phi_{\ell} \right\|_{\ell}^2 + \mathbf{1}_{\inf \rho_{\ell} > K} \cdot \rho_{\min}^{-1} \left\| [\rho_{\ell} - \bar{\rho}] \nabla_{\ell} \phi_{\ell} \right\|_{\ell}^2 \\
&\quad + \left\| \sqrt{\bar{\rho}} [\nabla \phi - \nabla_{\ell} \phi_{\ell}] \right\|_{\ell}^2 =: R_{\ell,1} + R_{\ell,2} + R_{\ell,3},
\end{aligned} \tag{6.10}$$

with K to be specified later. An analogous bound holds for $R_{\ell-1}$.

In order to treat $R_{\ell, \ell-1}$ (we drop the time dependence $t_{\leftarrow}^{\ell-1}$ for this term), we abbreviate $g := \sqrt{\bar{\rho}} \nabla \phi$ and perform the rewriting

$$\begin{aligned}
&\left(\sqrt{\bar{\rho}} e^{i\xi(\cdot)}, \nabla \phi \right)_{\ell} - \left(\sqrt{\bar{\rho}} e^{i\xi(\cdot)}, \nabla \phi \right)_{\ell-1} \\
&= \sum_{x \in G_{\ell-1, d}} h_{\ell-1}^d \left(e^{ix \cdot \xi} g(x) - \sum_{G_{\ell, d} \ni y \sim x} 3^{-d} e^{iy \cdot \xi} g(y) \right),
\end{aligned} \tag{6.11}$$

where $y \sim x$ indicates all points $y \in G_{\ell, d}$ such that $|y - x| \leq h_{\ell}$. In order to sum up over the frequencies ξ , we integrate by parts on the lattice $G_{\ell-1, d}$. More specifically, we rely on the increment relation

$$e^{i\xi \cdot (x + h e_j)} - e^{i\xi \cdot x} = e^{i\xi \cdot x} \underbrace{\left(e^{i\xi_j h} - 1 \right)}_{=: P(\xi_j h)}, \quad j \in \{1, \dots, d\}. \tag{6.12}$$

Take $\xi \neq 0$. Using (6.12) with the same increment $h = h_{\ell-1}$ in all sums of (6.11), we perform discrete integration by parts R times in direction j such that $\xi_j \neq 0$, and get

$$\begin{aligned}
&\left(\sqrt{\bar{\rho}} e^{i\xi(\cdot)}, \nabla \phi \right)_{\ell} - \left(\sqrt{\bar{\rho}} e^{i\xi(\cdot)}, \nabla \phi \right)_{\ell-1} \\
&= \left[\frac{-1}{P(\xi_j h)} \right]^R \sum_{x \in G_{\ell-1, d}} h_{\ell-1}^d \left(e^{ix \cdot \xi} \partial_{h, j}^R g(x) - \sum_{G_{\ell, d} \ni y \sim x} 3^{-d} e^{iy \cdot \xi} g(y) \partial_{h, j}^R g(y) \right),
\end{aligned} \tag{6.13}$$

where $\partial_{h,j}^R f(x) := \sum_{i=0}^R (-1)^i \binom{R}{i} f(x - ih e_j)$ is the standard backwards finite difference operator satisfying the relation

$$\partial_{h,j}^R f(x) = h^R \partial_j^R f(x) + h^{R+1} C(R) \partial^{R+1} f(\zeta), \quad \text{for some } \zeta = \zeta(x) \in \mathbb{T}^d. \quad (6.14)$$

By using the order-two bound $|f(x + h e_j) - 2f(x) + f(x - h e_j)| \lesssim h^2 \|f\|_{C^2}$ in the round bracket of (6.13) (with $f(x) := e^{i\xi \cdot x} \partial_{h,j}^R g(x)$), and the equivalence $\sin(z) \propto z$ for $z \in [-\pi/2, \pi/2]$, we rely on Assumptions A3–A4 to integrate by parts R times in all directions j with $\xi_j \neq 0$ (with R to be determined), and deduce

$$\begin{aligned} & \left| (\sqrt{\bar{\rho}} e^{i\xi(\cdot)}, \nabla \phi)_\ell - (\sqrt{\bar{\rho}} e^{i\xi(\cdot)}, \nabla \phi)_{\ell-1} \right| \\ & \leq \frac{1}{\left(\sum_{j=1}^d |P(\xi_j h_{\ell-1})| \right)^R} \sum_{y \in G_{\ell,d}} h_{\ell-1}^d \|g\|_{C^{R+3}} h_{\ell-1}^R h_{\ell-1}^2 |\xi|^4 \\ & \leq |\xi|^{4-R} \|g\|_{C^{R+3}} h_{\ell-1}^2, \end{aligned} \quad (6.15)$$

where we have also used (6.14) in the second-to-last inequality and the fact that $|P(\xi_j h)| = |\sin(\xi_j h/2)|, \forall j \in \{1, \dots, d\}$, in the last inequality. The estimate for $\xi = 0$ is even simpler, and requires no integration by parts at all. Provided $R > 4 + d/2$, (6.15) implies that we can sum up the terms making up $R_{\ell, \ell-1}$ in (6.9) and get

$$R_{\ell, \ell-1} \lesssim \|g\|_{C^{R+3}}^2 h_{\ell-1}^4. \quad (6.16)$$

Step 5: bounding $A_{I_\ell \setminus I_{\ell-1}}^2$ in (6.8). Dropping the dependence on t_{\leftarrow}^ℓ , we write

$$\begin{aligned} A_{I_\ell \setminus I_{\ell-1}} & \lesssim \sum_{\xi \in I_\ell \setminus I_{\ell-1}} \left| (\sqrt{\rho_\ell^\dagger} e^{i\xi(\cdot)}, \nabla_\ell \phi)_\ell - (\sqrt{\bar{\rho}} e^{i\xi(\cdot)}, \nabla \phi)_\ell \right|^2 \\ & \quad + \sum_{\xi \in I_\ell \setminus I_{\ell-1}} |(\sqrt{\bar{\rho}} e^{i\xi(\cdot)}, \nabla \phi)_\ell|^2 =: \bar{R}_\ell + \bar{R}_{I_\ell \setminus I_{\ell-1}}. \end{aligned} \quad (6.17)$$

The term \bar{R}_ℓ obviously has the same bound as the previously treated R_ℓ . Furthermore, as $R > 4 + d/2$, and reusing computations from (6.15), we get

$$\begin{aligned} \bar{R}_{I_\ell \setminus I_{\ell-1}} & \leq \sum_{\xi \in I_\ell \setminus I_{\ell-1}} \frac{1}{|P(\xi h_{\ell-1})|^{2R}} \|g\|_{C^R}^2 h_{\ell-1}^{2R} \\ & \leq \sum_{\xi \in I_\ell \setminus I_{\ell-1}} \frac{1}{|\xi|^{2R}} \|g\|_{C^R}^2 \leq \|g\|_{C^R}^2 h_{\ell-1}^4. \end{aligned} \quad (6.18)$$

Step 6: taking the expectations in (6.8). In order to bound $\mathbb{E}[R_{\ell,1}^2 + R_{\ell,2}^2]$, we consider the best estimate originating from picking either $K = \rho_{\min}/2$ or $K = \infty$ in (6.10): More precisely, using Hölder's inequality, Lemma 6.1, and the simple estimate $\|\bar{\rho} - \bar{\rho}_\ell\|_\ell \propto h_\ell^2 + \tau_\ell$, we obtain

$$\begin{aligned} & \mathbb{E}[R_{\ell,1}^2 + R_{\ell,2}^2] \\ & \lesssim_\varphi \min \left\{ \exp \left(-\frac{C \rho_{\min}}{\rho_{\max}^{1/2}} \left[\frac{N h_\ell^d}{\mu_\ell^2 \vee 1} \right]^{\frac{1}{2}} \right) \left[N^{-1} h_\ell^{-d} (\mu_\ell^2 \vee 1) \right] + \rho_{\min}^{-1} \left[N^{-1} h_\ell^{-d} (\mu_\ell^2 \vee 1) \right]^2; \right. \\ & \quad \left. \left[N^{-1} h_\ell^{-d} (\mu_\ell^2 \vee 1) \right] \right\} + \min \{ \rho_{\min}^{-2} (h_\ell^8 + \tau_\ell^4), h_\ell^4 + \tau_\ell^2 \}. \end{aligned}$$

As $\|\nabla\phi - \nabla_\ell\phi_\ell\| \propto h_\ell^2 + \tau_\ell$ (cfr. Lemma A.2), we get $\mathbb{E}[R_{\ell,3}^2] \leq C_\varphi(h_\ell^8 + \tau_\ell^4)$, and an analogous bound holds for $R_{\ell-1}$. Similar arguments (involving the same thresholds $K = \rho_{\min}/2$ or $K = \infty$), a Taylor expansion, and the discrete Parseval identity grant the estimate $R_{t_{\ell-1}^\ell, t_{\ell-1}^{\ell-1}} \lesssim_\varphi \min\{\rho_{\min}^{-1}\tau_\ell^2, \tau_\ell\}$.

Step 7: concluding the argument. Combining the estimates in Steps 4–6, we get

$$\begin{aligned} & \mathbb{E}\left[A_{I_{\ell-1}}^2 + A_{I_\ell \setminus I_{\ell-1}}^2\right] \\ & \lesssim_\varphi \min\left\{\exp\left(-\frac{C\rho_{\min}}{\rho_{\max}^{1/2}}\left[\frac{Nh_\ell^d}{\mu_\ell^2 \vee 1}\right]^{\frac{1}{2}}\right)\left[N^{-1}h_\ell^{-d}(\mu_\ell^2 \vee 1)\right] + \rho_{\min}^{-1}\left[N^{-1}h_\ell^{-d}(\mu_\ell^2 \vee 1)\right]^2;\right. \\ & \quad \left.\left[N^{-1}h_\ell^{-d}(\mu_\ell^2 \vee 1)\right]\right\} \\ & \quad + \min\{\rho_{\min}^{-2}(h_\ell^8 + \tau_\ell^4), h_\ell^4 + \tau_\ell^2\} + C(\rho_{\min})\{h_\ell^8 + \tau_\ell^4\}. \end{aligned}$$

Using the above inequality, (4.4), (6.4) and (6.6), we apply Gronwall's Lemma in (6.8) and conclude the proof.

Remark 6.2. The proof of Proposition 5.1 with Right-Most coupling is similar to the one we have provided for the Fourier coupling. The main adjustment concerns adapting the cross-variation structure (i.e., replacing the terms $A_{I_{\ell-1}} + A_{I_\ell \setminus I_{\ell-1}}$ in (6.7)). It is easy to see that that the term $A_{I_{\ell-1}} + A_{I_\ell \setminus I_{\ell-1}}$ in (6.7) is replaced by

$$\begin{aligned} & \sum_{x \in G_{\ell,d}} h_\ell^d \rho_{h_\ell}^+(x) |\nabla_{h_\ell} \phi_{h_\ell}(x)|^2 + \sum_{x \in G_{\ell-1,d}} h_{\ell-1}^d \rho_{h_{\ell-1}}^+(x) |\nabla_{h_{\ell-1}} \phi_{h_{\ell-1}}(x)|^2 \\ & \quad - 2 \sum_{y \in B_{\ell-1}^+(x)} \sum_{x \in G_{\ell-1,d}} h_\ell^d \sqrt{\rho_{h_\ell}^+(y)} \nabla_{h_\ell} \phi_{h_\ell}(y) \cdot \sqrt{\rho_{h_{\ell-1}}^+(x)} \nabla_{h_{\ell-1}} \phi_{h_{\ell-1}}(x) \\ & = \sum_{y \in B_{\ell-1}^+(x)} \sum_{x \in G_{\ell-1,d}} h_\ell^d \left| \sqrt{\rho_{h_\ell}^+(y)} \nabla_{h_\ell} \phi_{h_\ell}(y) - \sqrt{\rho_{h_{\ell-1}}^+(x)} \nabla_{h_{\ell-1}} \phi_{h_{\ell-1}}(x) \right|^2. \end{aligned} \quad (6.19)$$

From (6.19), it is relatively straightforward to get the Err_{num} contribution using similar techniques to those deployed in (6.10) (i.e., choosing the best cutoff for the square-root between $K = \rho_{\min}/2$ and $K = \infty$). All other components of the estimate do not change with respect to the proof in the Fourier case.

Remark 6.3. Having two separate estimates originating from two cut-off values $K = \rho_{\min}/2$ or $K = \infty$ helps providing a reliable estimate for Err_{num} in (5.1): However, these two estimates can – in many cases – still be substantially suboptimal, as they do not rely on the local structure of the mean field limit $\bar{\rho}$. A relevant example is discussed in our simulations in Section 7.

6.2. Proof of Theorem 5.3. We only provide the proof for the Fourier coupling (the proof is entirely analogous in the case of Right-Most coupling). Since K is big enough in Assumption A1, the error Err_{mod} in (5.1) is dominated by $N^{-1}h_\ell^{-d}(\mu_\ell^2 \vee 1)$. Using (4.1),

(5.1), (5.2), and the definition of μ_ℓ , we deduce

$$\begin{aligned}
\text{Var} [\mu_{MLMC}] &\lesssim M_{\ell_0}^{-1} + \sum_{\ell=\ell_0+1}^L M_\ell^{-1} [N^{-1}h_\ell^{-d}(\mu_\ell^2 \vee 1) + h_\ell^4 + \tau_\ell^2] \\
&\lesssim M_{\ell_0}^{-1} + \sum_{\ell=\ell_0+1}^L \frac{\tau_{\min}}{\tau_\ell} h_{\min}^d [N^{-1}h_\ell^{-2d}(\mu_\ell^2 \vee 1) + h_\ell^{4-d}(\mu_\ell^2 \vee 1)] \\
&\lesssim M_{\ell_0}^{-1} + \sum_{\ell=\ell_0+1}^L \frac{\tau_{\min}}{\tau_\ell} h_{\min}^d h_\ell^{(4 \wedge \alpha) - d}. \tag{6.20}
\end{aligned}$$

The choice $L - \ell_0 \propto |\log(h_{\min})|$ implies that $M_{\ell_0}^{-1} \lesssim h_{\min}^d$. In the case $(\alpha \wedge 4) \geq d$, we can continue in (6.20) as

$$\text{Var} [\mu_{MLMC}] \lesssim h_{\min}^d + \sum_{\ell=\ell_0+1}^L \frac{\tau_{\min}}{\tau_\ell} h_{\min}^d,$$

and (5.4) is proved. If instead $(\alpha \wedge 4) < d$, we can write

$$\text{Var} [\mu_{MLMC}] \lesssim h_{\min}^d + \sum_{\ell=\ell_0+1}^L \frac{\tau_{\min}}{\tau_\ell} h_{\min}^{(\alpha \wedge 4)} \kappa_x^{\ell((\alpha \wedge 4) - d)},$$

and (5.4) again follows. Proving (5.5) is immediate. Finally, the speed-up factor (5.6) can be readily deduced by: (i) taking into account an adaptation of the systematic error estimate of [7, Theorem 2] to the full space/time discretisation (this is obtained using similar techniques to the ones deployed in the proof of Proposition 5.1); (ii) dividing the cost of a standard Monte Carlo estimator with the same variance as μ_{MLMC} (see (5.4)), which is $\text{Cost}_{MC} \propto h_{\min}^{-(\alpha \wedge 4 \wedge d)} \cdot h_{\min}^{-d} \cdot \tau_{\min}^{-1}$, and the cost of the Multilevel Monte Carlo method (5.5). Theorem 5.3 is thus proved.

7. NUMERICAL SIMULATIONS

We provide numerical simulations demonstrating the validity of our theoretical results in the two dimensional case.

7.1. **Setting.** The precise details of our setting are as follows:

- Initial condition for mean-field dynamics: we use two different initial conditions. The first one

$$\bar{\rho}_{0,reg} = Z_{reg}^{-1} \left(1 + e^{-(\sin^2(x-\pi/2) + \sin^2(y-3\pi/2))/2} / (\sqrt{2\pi}) \right) \tag{7.1}$$

– where Z_{reg} is the normalising constant – is bounded away from zero, and with relatively low ratio $\sqrt{\rho_{\max}}/\rho_{\min} \approx 13.4$. The second initial condition

$$\bar{\rho}_{0,irreg} = Z_{irreg}^{-1} e^{-(\sin^2(x-\pi/2) + \sin^2(y-3\pi/2))/(2 \cdot 0.1)} / (\sqrt{2\pi \cdot 0.1}) \tag{7.2}$$

has ultra-low density regions, and much larger ratio $\sqrt{\rho_{\max}}/\rho_{\min} \gg 10^6$. The two initial conditions are shown in Figure 1.

- Time-stepping: we stick to a simple explicit Euler-Maruyama scheme, i.e., we pick $a_0 = 1, a_1 = -1, b_0 = 0, b_1 = 1$ in (2.1).

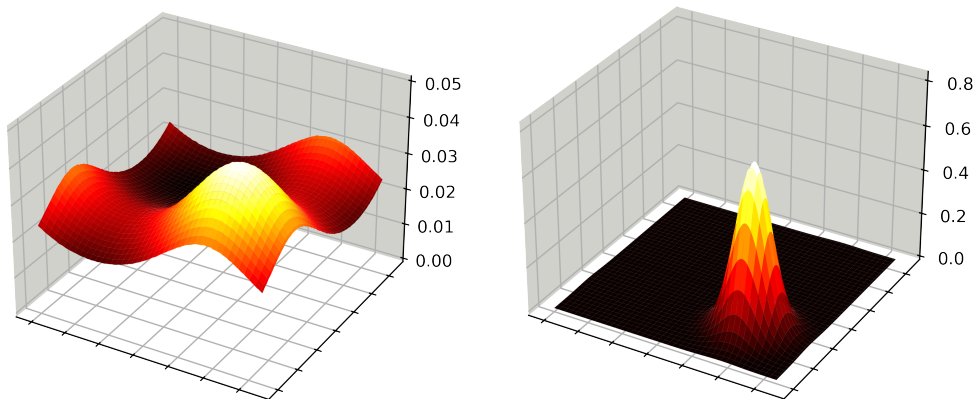


FIGURE 1. *Left*: 3d heat map of $\bar{\rho}_{0,reg}$; *Right*: 3d heat map of $\bar{\rho}_{0,irreg}$

- Multilevel Monte Carlo discretisation: we consider at most $L = 6$ levels, and use Right-Most neighbour coupling, see Subsection 3.2. When $L = 6$, for the finest level in space, each axis is split in $2^7 = 128$ parts, i.e., $h_{\min} = 2\pi \cdot 2^{-7} \approx 0.05$. Furthermore, the finest level in time has time-step $t_{\min} = 10^{-3}$. Consecutive levels are designed to preserve the CFL condition: specifically, we choose $h_{\ell-1} = 2h_{\ell}$ and $\tau_{\ell-1} = 4\tau_{\ell}$, so that $\mu_{\ell} = \tau_{\ell}/h_{\ell}^2$ is constant over ℓ . Furthermore, the number of samples quadruples with each level change, i.e., $M_{\ell-1} = 4M_{\ell}$. This is also expected to give the cost ratio (5.6).

For qualitative illustration purposes, we show snapshots of a given trajectory of (2.1) in Figures 2–3 (3d heat maps) and Figures 4–5 (2d heat maps)¹.

- Time domain: we run simulations on the interval $[0, 2^{10} \cdot t_{\min}] = [0, 1024 \text{ ms}]$.
- Differential operators: the second-order operators used in (2.1) are

$$\Delta_h f_h(x) := \frac{-4f_h(x) + \sum_{y \sim x} f_h(y)}{h^2},$$

$$\nabla_h \cdot f_h(x) := \sum_{r=1}^d \frac{[f_h]_r(x + hf_r) - [f_h]_r(x - hf_r)}{2h}$$

with $y \sim x$ meaning that x, y are adjacent grid points.

- Test functions: we use $\psi(x) := x^2$ and $\phi(x) := \sin(x) + \sin(y)$.

7.2. Numerical results. We report quantitative results of the simulations for

- $N = 2 \cdot 10^9$ and $\rho_0 = \bar{\rho}_{0,reg}$ (Figure 6),
- $N = 2 \cdot 10^9$ and $\rho_0 = \bar{\rho}_{0,irreg}$ (Figure 7),
- $N = 2 \cdot 10^7$ and $\rho_0 = \bar{\rho}_{0,reg}$ (Figure 8), and
- $N = 2 \cdot 10^5$ and $\rho_0 = \bar{\rho}_{0,reg}$ (Figure 9).

¹The graphics commands used to generate Figures 4–5 are based on the code in [this example](#).

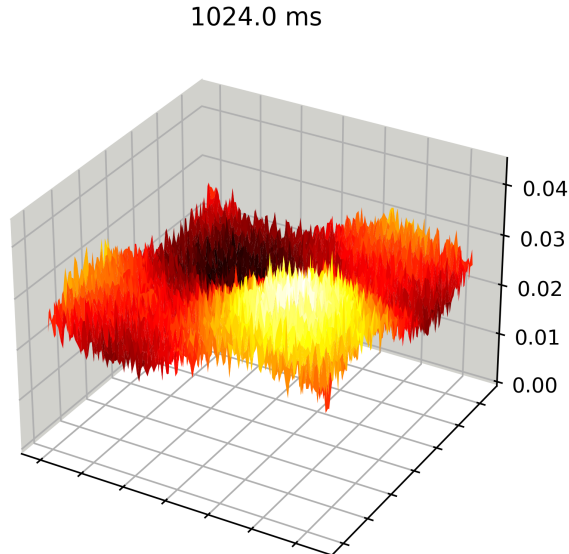


FIGURE 2. 3d snapshots at time $T = 1024 \text{ ms}$ of a trajectory of the discrete Dean–Kawasaki equation (2.1) started from $\bar{\rho}_{0,reg}$, and with $N = 2 \cdot 10^6$ particles, on finest level ($h = 2\pi \cdot 2^{-7}$, $\tau = 0.001$).

Figures 6, 7, 8, 9 are made of four plots, namely: variance estimate across levels (Top-Left), expected value estimate across levels (Top-Right), time-dependent estimate of expected value for MC, MLMC, and – whenever not too expensive to simulate – Brownian particle system (Bottom-Left), cost ratio between MC and MLMC for varying h_{\min} (Bottom-Right).

We summarise our findings.

7.2.1. *Variance estimates.* The quadratic decay $O(h_\ell^2)$ for $\text{Var}[P_\ell - P_{\ell-1}]$ in (5.1) is clearly visible for the simulation with either $N = 2 \cdot 10^9$ or $N = 2 \cdot 10^7$, started from $\rho_0 = \bar{\rho}_{0,reg}$ (Figures 6 and Figures 8). The same clear decay also holds in the case $N = 2 \cdot 10^9$ and $\rho_0 = \bar{\rho}_{0,irreg}$ (Figure 7), even though (5.1) would only predict linear decay $O(h_\ell)$ in this case. The reason for the better-than-expected result (cfr. Remark 6.3), is likely to be the specific nature of the mean-field limit, in which areas of low density coincide with areas of low gradient values, thus making the constant multiplying the quadratic contributions sufficiently low so as to win over linear decay. When N is decreased to $N = 2 \cdot 10^5$ (with $\rho_0 = \bar{\rho}_{0,reg}$), the quadratic decay breaks down for the lowest value of h (Figure 9): this is to be expected from (5.1), as the contribution $\propto N^{-1}h_\ell^{-2}$ starts dominating over the numerical error $\propto h_\ell^2$ at this point.

7.2.2. *Expected values estimates.* Quadratic decay $O(h_\ell^2)$ for $\mathbb{E}[P_\ell - P_{\ell-1}]$ is clearly visible in Figures 6, 8, where $N = 2 \cdot 10^9$, and to a good extent also when $N = 2 \cdot 10^7$ (Figure 8)

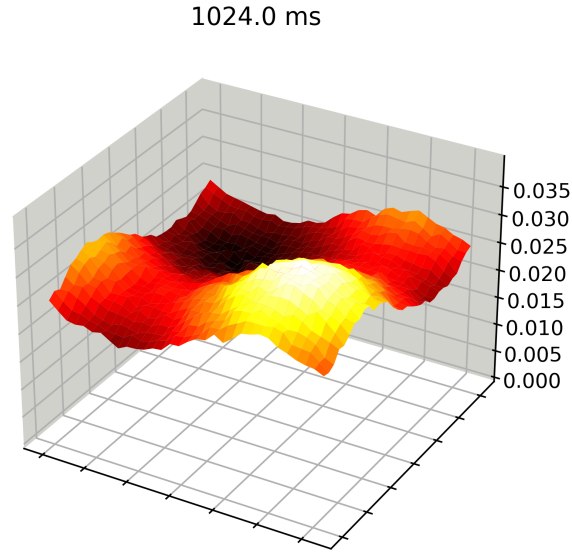


FIGURE 3. Same setting as in Figure 2, but on coarser level ($h = 2\pi \cdot 2^{-5}, \tau = 0.001 \cdot 4^2$).

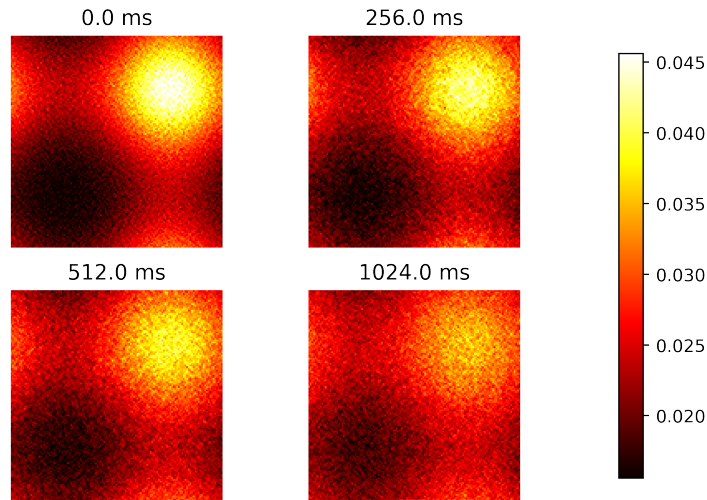


FIGURE 4. 2d snapshots of a trajectory of the discrete Dean–Kawasaki equation (2.1) started from $\bar{\rho}_{0,reg}$ and with $N = 2 \cdot 10^6$ particles, and on finest level ($h = 2\pi \cdot 2^{-7}, \tau = 0.001$)

and when $N = 2 \cdot 10^5$ (Figure 9). This is consistent with the results showed in [7], and validates the systematic error of our method.

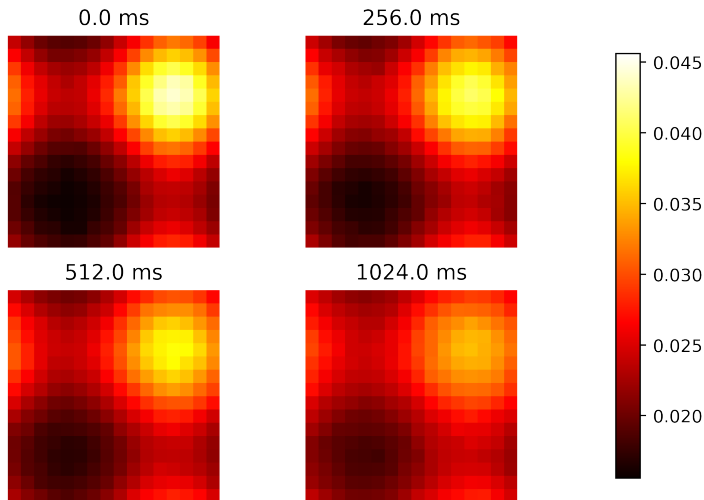


FIGURE 5. Same setting as in Figure 4, but on coarser level ($h = 2\pi \cdot 2^{-4}, \tau = 0.001 \cdot 4^3$).

7.2.3. *Time convergence for MC, MLMC, and particle dynamics.* We plot the estimate for $\mathbb{E}[P]$ at different points in time for the MC and MLMC methods, as well as also for the particle system whenever this is not too costly to simulate (i.e., in the simulations with $N = 2 \cdot 10^5$ or $N = 2 \cdot 10^7$). As foreseen, the expected value as computed by MLMC stabilises more quickly compared to MC. When $N = 2 \cdot 10^5$, one can see the rapid alignment of the expected values as computed using the particle system and MLMC. When $N = 2 \cdot 10^7$, one can see that the estimate produced by MLMC stabilises before the one given by the particle system: This is consistent with keeping the computing time fixed, and the increased simulation cost for the particles (this leads to fewer samples of the particle system over the same amount of time).

7.2.4. *Cost reduction of MLMC over MC.* In all cases with the exception of the simulation with $N = 2 \cdot 10^5$, there is clear agreement between the cost ratio between MC/MLMC methods, and its maximum predicted growth $O(h_{\min}^{-2} |\log_2(h_{\min})|^{-1})$ (see Theorem 5.3, logarithmic correction is introduced by choice of realisation M_ℓ in Section 7.1). The cost ratios for the simulations with $N = 2 \cdot 10^7$ and $N = 2 \cdot 10^9$ started from $\rho_0 = \bar{\rho}_{0,reg}$ are roughly the same, as it should be since in both cases the variance decay is almost perfectly quadratic and the initial datum is the same. For $N = 2 \cdot 10^5$, the agreement between actual and predicted speed-up factor $O(h_{\min}^{-2} |\log_2(h_{\min})|^{-1})$ breaks down for the smallest value of h_{\min} , and this is consistent with the quadratic variance bound being violated for the same value of h_{\min} .

APPENDIX A. ESTIMATES FOR FULLY DISCRETE SETTING

In what follows, it is convenient to use the short-hand notation $\mu := \tau/h^2$ for the standard CFL quotient.

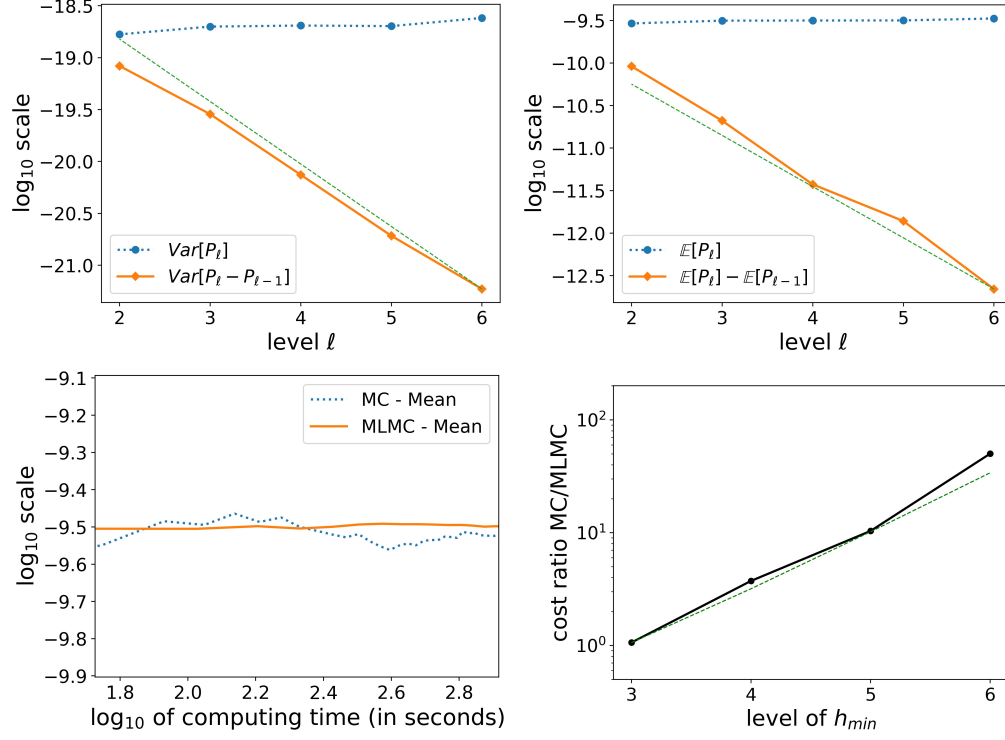


FIGURE 6. Experimental results ($N = 2 \cdot 10^9$, $\bar{\rho}_0 = \bar{\rho}_{0,reg}$). Green dashed line corresponds to decay $O(h_\ell^2)$ in Top-Left/Top-right plots, and to growth $O(h_\ell^{-2} |\log_2(h_\ell)|^{-1})$ in Bottom-Right plot.

Lemma A.1 (Discrete energy estimates). *We define the test function dynamics*

$$\phi_{h,\tau}^{m\tau} = A_h \phi_{h,\tau}^{(m+1)\tau}, \quad (\text{A.1})$$

with $A_h := (I_d - \tau b_0 \frac{1}{2} \Delta_h)^{-1} (I_d + \tau b_1 \frac{1}{2} \Delta_h)$, and where b_0, b_1 are the coefficients from (2.1), see also Assumption A2. If $b_1 > b_0$, the energy estimate for $\phi_{h,\tau}$

$$\tau \sum_m \|\nabla_h \phi_{h,\tau}^{m\tau}\|_h^2 \lesssim (\mu^2 \wedge 1) \|\phi_{h,\tau}^T\|_h^2 \quad (\text{A.2})$$

holds subject to μ being sufficiently small. If $b_1 \leq b_0$, then (A.2) holds with no smallness requirement on μ .

Proof. We multiply both sides in (A.1) by $(I_d - \tau \frac{b_0}{2} \Delta_h)$, compute the $\|\cdot\|_h^2$ norm of both resulting sides, reshuffle the terms, and obtain

$$\begin{aligned} & b_0 \tau \|\nabla_h \phi_{h,\tau}^{m\tau}\|_h^2 + b_1 \tau \|\nabla_h \phi_{h,\tau}^{(m+1)\tau}\|_h^2 \\ &= \|\phi_{h,\tau}^{(m+1)\tau}\|_h^2 - \|\phi_{h,\tau}^{m\tau}\|_h^2 + \tau^2 \frac{b_1^2}{4} \|\Delta_h \phi_{h,\tau}^{(m+1)\tau}\|_h^2 - \tau^2 \frac{b_0^2}{4} \|\Delta_h \phi_{h,\tau}^{m\tau}\|_h^2. \end{aligned}$$

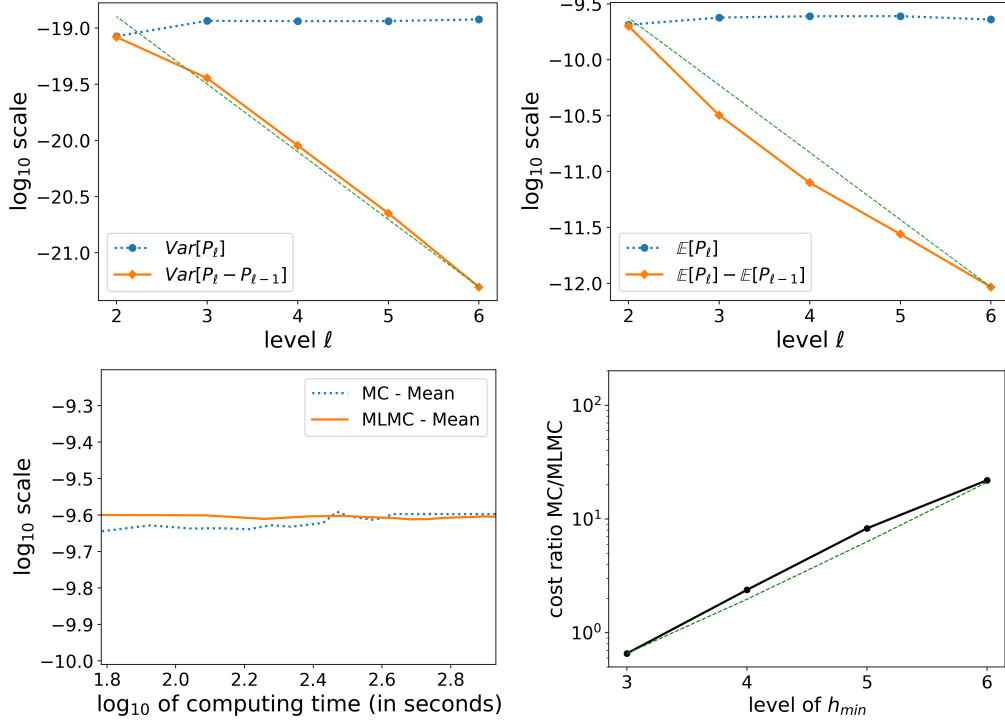


FIGURE 7. Experimental results ($N = 2 \cdot 10^9$, $\bar{\rho}_0 = \bar{\rho}_{0,irreg}$). Green dashed line corresponds to decay $O(h_\ell^2)$ in Top-Left/Top-right plots, and to growth $O(h_\ell^{-2} |\log_2(h_\ell)|^{-1})$ in Bottom-Right plot.

Summing over m , we control the sum of the contributions $\tau^2(b_1^2/4)\|\Delta_h\phi_{h,\tau}^{(m+1)\tau}\|_h^2 - \tau^2(b_0^2/4)\|\Delta_h\phi_{h,\tau}^{m\tau}\|_h^2$ by using a telescopic argument if $b_1 \leq b_0$, or by absorbing the term $\tau^2(b_1^2/4)\|\Delta_h\phi_{h,\tau}^{(m+1)\tau}\|_h^2$ in the term $b_1\tau\|\nabla_h\phi_{h,\tau}^{(m+1)\tau}\|_h^2$ (subject to μ being sufficiently small) if instead $b_1 > b_0$. In all cases, (A.2) follows by additionally using that $b_1^2\tau^2\|\Delta_h\phi_{h,\tau}^T\|_h \lesssim \mu^2\|\phi_{h,\tau}^T\|_h^2$. \square

Lemma A.2 (Error estimates for standard heat equation, cfr. [23]). *Let ϕ satisfy the continuous backwards heat equation ending in $\phi^T = \varphi \in C^2$, and let $\phi_{h,\tau}$ satisfy the discrete backwards heat equation (A.1) ending in $\mathcal{I}_h\varphi$. Then, for all m , we have*

$$\|\phi(\cdot, m\tau) - \phi_{h,\tau}^{m\tau}\|_\infty \lesssim h^2 + \tau. \quad (\text{A.3})$$

Lemma A.3. *For any discrete function $\phi_h \in H_h^2$, we have*

$$\|\nabla_h [(I_d - b_0\tau\Delta_h)^{-1}\phi_h - \phi_h]\|_h^2 \lesssim b_0^2\tau^2\|\phi_h\|_{H_h^2}^2. \quad (\text{A.4})$$

Proof. This follows by taking the Fourier transform of $y_h := (I_d - b_0\tau\Delta_h)^{-1}\phi_h$, which gives $\hat{y}_h(\xi) - \hat{\phi}_h(\xi) \propto (\tau P(\xi)\hat{\phi}_h(\xi))/(1 + \tau P(\xi))$ for some $P(\xi) \propto |\xi|^2$. \square

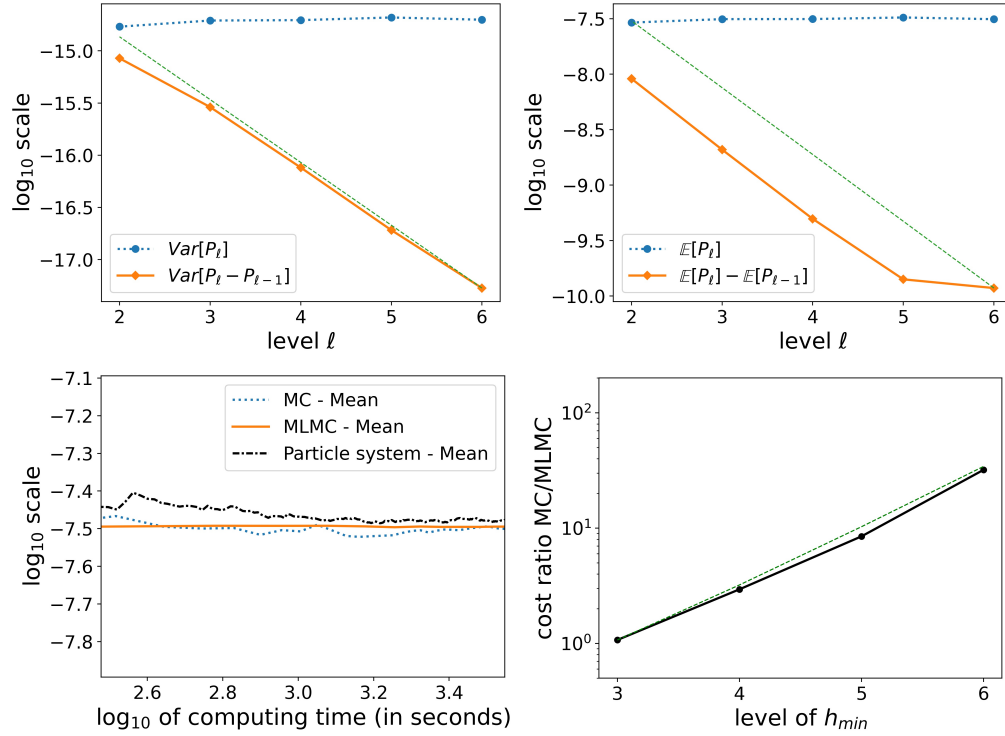


FIGURE 8. Experimental results ($N = 2 \cdot 10^7$, $\bar{\rho}_0 = \bar{\rho}_{0,reg}$). Green dashed line corresponds to decay $O(h_\ell^2)$ in Top-Left/Top-right plots, and to growth $O(h_\ell^{-2} |\log_2(h_\ell)|^{-1})$ in Bottom-Right plot.

Lemma A.4 (Martingale property for discrete fluctuations). *Let (A.1) be the dynamics for the test function $\phi_{h,\tau}$. Let $\rho_{h,\tau}$ be the solution to (2.1). Then $(\rho_{h,\tau}, \phi_{h,\tau})_h$ is a discrete time martingale.*

Proof. The definition of A_h entails that $\rho_{h,\tau}^{(m+1)\tau} = A_h \rho_{h,\tau}^{m\tau} + \mathcal{M}_m$, where \mathcal{M}_m encodes the noise. Using the symmetry of A_h and (A.1), we end the proof by writing

$$\begin{aligned} (\rho_{h,\tau}^{(m+1)\tau}, \phi_{h,\tau}^{(m+1)\tau})_h &= (A_h \rho_{h,\tau}^{m\tau} + \mathcal{M}_m, \phi_{h,\tau}^{(m+1)\tau})_h \\ &= (\rho_{h,\tau}^{m\tau}, A_h \phi_{h,\tau}^{(m+1)\tau})_h + (\mathcal{M}_m, \phi_{h,\tau}^{(m+1)\tau})_h \\ &= (\rho_{h,\tau}^{m\tau}, \phi_{h,\tau}^{m\tau})_h + (\mathcal{M}_m, \phi_{h,\tau}^{(m+1)\tau})_h. \end{aligned} \quad \square$$

APPENDIX B. PROOF OF LEMMA 6.1

We need the following simple estimate.

Lemma B.1. *Let $C > 0$ be constant. Then, for $\alpha \geq 1$ and $\beta > 0$, it holds*

$$\int_0^\infty \exp\{-\alpha x^{1/\beta} / \sqrt{1+x^{1/\beta}}\} dx \leq C \alpha^{-\beta}.$$

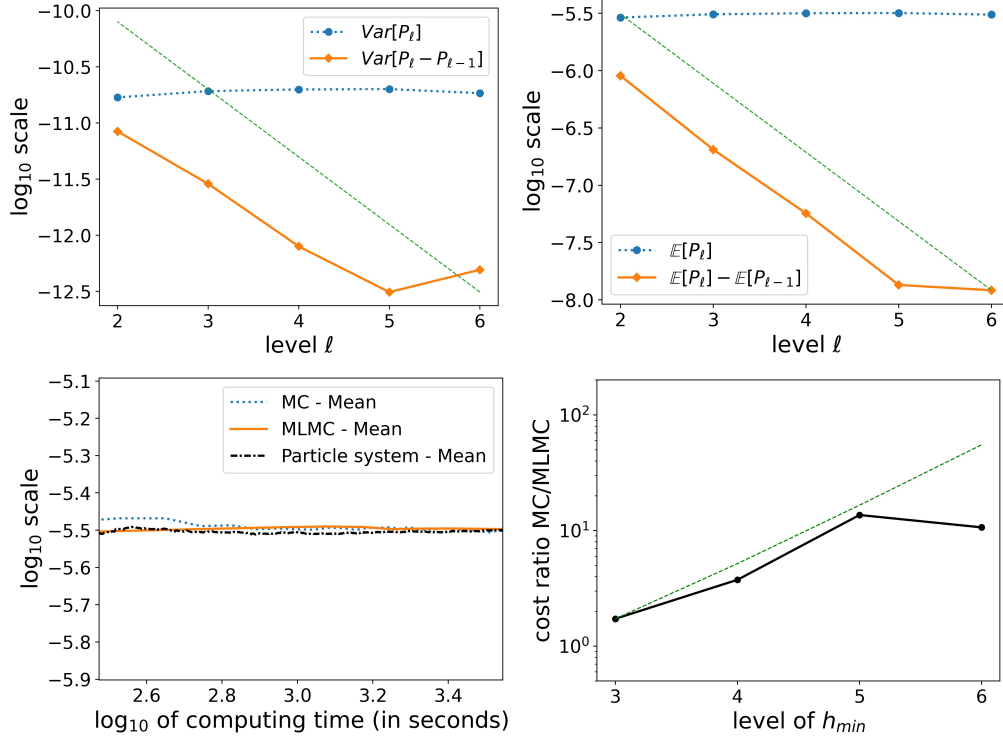


FIGURE 9. Experimental results ($N = 2 \cdot 10^5$, $\bar{\rho}_0 = \bar{\rho}_{0,reg}$). Green dashed line corresponds to decay $O(h_\ell^2)$ in Top-Left/Top-right plots, and to growth $O(h_\ell^{-2} |\log_2(h_\ell)|^{-1})$ in Bottom-Right plot.

Proof. Using the inequality $1 + x^{1/\beta} \leq x^{1/\beta}(1 + \alpha)$ (valid for $x \geq \alpha^{-\beta}$) we write

$$\begin{aligned} & \int_0^{\alpha^{-\beta}} \exp\left\{-\alpha \frac{x^{1/\beta}}{\sqrt{1+x^{1/\beta}}}\right\} dx + \int_{\alpha^{-\beta}}^{\infty} \exp\left\{-\alpha \frac{x^{1/\beta}}{\sqrt{1+x^{1/\beta}}}\right\} dx \\ & \lesssim_{\beta} \alpha^{-\beta} + \int_0^{\infty} \exp\{-C\sqrt{\alpha}y^2\} y^{4\beta-1} dy \lesssim_{\beta} \alpha^{-\beta}, \end{aligned}$$

where we used the bound $z/\sqrt{1+\alpha} \geq \sqrt{\alpha}/\sqrt{2}$ (for $\alpha \geq 1$) and a change of variables in the second-to-last inequality, and Gaussian moment bounds in the last inequality. \square

Proof of Lemma 6.1. Let $x \in G_{h,d}$ and $t \in \mathcal{S}_\tau$ be fixed. Let φ_h be the discrete Dirac delta in x , namely $\varphi_h := \delta_{y \equiv x} h^{-d/2}$. Moreover, let $\phi_{h,\tau}$ be given by the discrete backwards heat equation (A.1), and with final datum $\phi_{h,\tau}^t = \varphi_h$. We define the stopping time $T_\circ := \min\{s \in \mathcal{S}_\tau : \|\rho_{h,\tau}^s - \bar{\rho}_{h,\tau}^s\|_\infty \geq B\rho_{\min}/2\}$. Let $j \in \mathbb{N}$ be even. The same exact reasoning as in Step 3 from the proof of Proposition 5.1 allows to define a continuous-time martingale D^s such that $D^s = (\rho_{h,\tau}^s - \bar{\rho}_{h,\tau}^s, \phi_{h,\tau}^s)_h$ for all $\mathcal{S}_\tau \ni s \leq t$. Using the continuous Itô formula, the bound $\lambda_{\max}(I_d - b_0\tau\Delta_h)^{-1} \leq 1$, the definition of T_\circ , and

the notation $s_{\leftarrow} := \max\{m \in \mathcal{S}_\tau : m < s\}$, we obtain

$$\begin{aligned} \mathbb{E}[(D^{t \wedge T_\circ})^j] &\leq \mathbb{E}[(D^0)^j] + \frac{j^2}{N} \mathbb{E} \left[\int_0^{t \wedge T_\circ} (D^s)^{j-2} ([\rho_{h,\tau}^{s_{\leftarrow}}]^+, |\nabla_h \phi_{h,\tau}^{s_{\leftarrow}}|^2)_h ds \right] \\ &\lesssim \mathbb{E}[\|\rho_{h,\tau}^0 - \bar{\rho}_{h,\tau}^0\|_\infty^j] \|\phi_{h,\tau}^0\|_{L^1}^j \\ &\quad + \frac{j^2}{N} \mathbb{E} \left[\sup_{s \leq t \wedge T_\circ} (D^s)^{j-2} \right] \rho_{\max}(B+1) \sum_{s \in \mathcal{S}_\tau, s < t \wedge T_\circ} \|\nabla_h \phi_{h,\tau}^s\|_h^2 \tau. \end{aligned}$$

Lemma A.1 with the fact that $\|\phi_{h,\tau}^t\|^2 \propto h^{-d}$, and Doob' martingale inequality imply

$$\begin{aligned} \mathbb{E} \left[\sup_{s \leq t \wedge T_\circ} (D^s)^j \right] &\lesssim \mathbb{E}[(D^{t \wedge T_\circ})^j] \\ &\leq (N^{-1}h^{-d})^{\frac{j}{2}} + N^{-1}j^2 \mathbb{E} \left[\sup_{s \leq t \wedge T_\circ} (D^s)^{j-2} \right] \rho_{\max}(B+1)(\mu^2 \vee 1)h^{-d}. \end{aligned}$$

Using Hölder and Young inequalities with conjugate exponents $j/2, j/(j-2)$ and absorbing the term $\mathbb{E}[\sup_{s \leq t \wedge T_\circ} (D^s)^j]$, we arrive at

$$\mathbb{E} \left[\left(\rho_{h,\tau}^{t \wedge T_\circ} - \bar{\rho}_{h,\tau}^{t \wedge T_\circ}, \phi_{h,\tau}^{t \wedge T_\circ} \right)_h^j \right]^{2/j} \lesssim C j^2 \frac{(B+1)\rho_{\max}(\mu^2 \vee 1)}{N h^d}. \quad (\text{B.1})$$

Chebyshev's inequality and an optimisation in j then imply

$$\mathbb{P} \left[\sup_{s \leq t \wedge T_\circ} |D^s| \geq \frac{B\rho_{\min}}{4} \right] \leq \exp \left(-\frac{C\rho_{\min}}{\rho_{\max}^{1/2}} \cdot \left\{ \frac{N h^d}{\mu^2 \vee 1} \right\}^{1/2} \cdot \frac{B}{\sqrt{B+1}} \right).$$

Using the definition of D^s , we then obtain

$$\begin{aligned} \mathbb{P} \left[t \leq T_\circ, |\rho_{h,\tau}^t - \bar{\rho}_{h,\tau}^t|(x) \geq \frac{B\rho_{\min}}{4} \right] \\ \leq \exp \left(-\frac{C\rho_{\min}}{\rho_{\max}^{1/2}} \cdot \left\{ \frac{N h^d}{\mu^2 \vee 1} \right\}^{1/2} \cdot \frac{B}{\sqrt{B+1}} \right), \end{aligned} \quad (\text{B.2})$$

and (6.1) follows from applying (B.2) over the union of all $(t, x) \in \mathcal{S}_\tau \times G_{h,d}$.

Assume now that $\alpha := C[\rho_{\min}/\rho_{\max}^{1/2}]\{N h^d/(\mu^2 \vee 1)\}^{1/2} \geq 1$. Then the inequality (6.2) is deduced from (6.1) using the equality $\mathbb{E}[X] = \int_0^\infty \mathbb{P}(X \geq x) dx$ (which is valid for every non-negative real-valued random variable X), a simple change of variables, and Lemma B.1 with the aforementioned α . Namely,

$$\begin{aligned} \mathbb{E} \left[\sup_{t \in \mathcal{S}_\tau} \|\rho_{h,\tau}^t - \bar{\rho}_{h,\tau}^t\|_\infty^j \right] &= \int_0^\infty \mathbb{P} \left(\sup_{t \in \mathcal{S}_\tau} \|\rho_{h,\tau}^t - \bar{\rho}_{h,\tau}^t\|_\infty^j \geq x \right) dx \\ &= \int_0^\infty \mathbb{P} \left(\sup_{t \in \mathcal{S}_\tau} \|\rho_{h,\tau}^t - \bar{\rho}_{h,\tau}^t\|_\infty \geq B^{1/j} \rho_{\min} \right) \rho_{\min}^j dB \\ &\lesssim (C(\rho_{\min}/\rho_{\max}^{1/2})[N h^d/(\mu^2 \vee 1)]^{1/2})^{-j} \rho_{\min}^j. \end{aligned}$$

Adapting the proof of (6.2) in the case $\alpha < 1$ so as to get a bound which is independent of ρ_{\min} can be done by replicating the analysis leading up to (B.2) by replacing ρ_{\min} with ρ_{\max} in the definition of the stopping time T_\circ and all relevant thresholds (we omit the details). Finally, (6.3) is easily proved along the lines of [7, Lemma 16]. \square

Data availability statement. The datasets generated and analyzed during the current study are available from the corresponding author on reasonable request.

Conflict of interest. The authors have no relevant financial or non-financial interest to disclose.

Acknowledgments. Both authors gratefully acknowledge funding from the Austrian Science Fund (FWF) through the project F65. Furthermore, both authors wish to thank Quinn Winters for useful preliminary discussions on the subject of this paper.

REFERENCES

- [1] A. Barth, C. Schwab, and N. Zollinger. Multi-level Monte Carlo finite element method for elliptic PDEs with stochastic coefficients. *Numer. Math.*, 119(1):123–161, 2011. ISSN 0029-599X,0945-3245. doi:[10.1007/s00211-011-0377-0](https://doi.org/10.1007/s00211-011-0377-0).
- [2] A. Barth, A. Lang, and C. Schwab. Multilevel Monte Carlo method for parabolic stochastic partial differential equations. *BIT*, 53(1):3–27, 2013. ISSN 0006-3835,1572-9125. doi:[10.1007/s10543-012-0401-5](https://doi.org/10.1007/s10543-012-0401-5).
- [3] A. Brandt, M. Galun, and D. Ron. Optimal multigrid algorithms for calculating thermodynamic limits. *Journal of Statistical Physics*, 74:313–348, 1994. doi:[10.1007/BF02186816](https://doi.org/10.1007/BF02186816).
- [4] J. Charrier, R. Scheichl, and A. L. Teckentrup. Finite element error analysis of elliptic PDEs with random coefficients and its application to multilevel Monte Carlo methods. *SIAM J. Numer. Anal.*, 51(1):322–352, 2013. ISSN 0036-1429,1095-7170. doi:[10.1137/110853054](https://doi.org/10.1137/110853054).
- [5] F. Chung and L. Lu. Concentration inequalities and martingale inequalities: a survey. *Internet mathematics*, 3(1):79–127, 2006.
- [6] K. A. Cliffe, M. B. Giles, R. Scheichl, and A. L. Teckentrup. Multilevel Monte Carlo methods and applications to elliptic PDEs with random coefficients. *Comput. Vis. Sci.*, 14(1):3–15, 2011. ISSN 1432-9360,1433-0369. doi:[10.1007/s00791-011-0160-x](https://doi.org/10.1007/s00791-011-0160-x).
- [7] F. Cornalba and J. Fischer. The Dean–Kawasaki equation and the structure of density fluctuations in systems of diffusing particles. *Arch. Rational Mech. Anal.*, 247(76), 2023. doi:[10.1007/s00205-023-01903-7](https://doi.org/10.1007/s00205-023-01903-7).
- [8] F. Cornalba, J. Fischer, J. Ingmanns, and C. Raithel. Density fluctuations in weakly interacting particle systems via the dean-kawasaki equation. *Preprint*, 2023. URL <https://arxiv.org/abs/2303.00429>.
- [9] M. Croci, M. B. Giles, M. E. Rognes, and P. E. Farrell. Efficient white noise sampling and coupling for multilevel monte carlo with nonnested meshes. *SIAM/ASA Journal on Uncertainty Quantification*, 6(4):1630–1655, 2018. doi:[10.1137/18M1175239](https://doi.org/10.1137/18M1175239).
- [10] N. Dirr, B. Fehrman, and B. Gess. Conservative stochastic PDE and fluctuations of the symmetric simple exclusion process. *Preprint*, 2020. URL <https://arxiv.org/abs/2012.02126>.
- [11] A. Djurdjevac, H. Kremp, and N. Perkowski. Weak error analysis for a nonlinear spde approximation of the dean-kawasaki equation. *Preprint*, 2022. URL <https://arxiv.org/abs/2212.11714>.
- [12] B. Fehrman and B. Gess. Large deviations for conservative stochastic PDE and non-equilibrium fluctuations. *Preprint*, 2019. URL <https://arxiv.org/abs/1910.11860>.

- [13] M. B. Giles. Multilevel Monte Carlo path simulation. *Oper. Res.*, 56(3):607–617, 2008. ISSN 0030-364X,1526-5463. doi:[10.1287/opre.1070.0496](https://doi.org/10.1287/opre.1070.0496).
- [14] M. B. Giles. Multilevel Monte Carlo methods. *Acta Numer.*, 24:259–328, 2015. ISSN 0962-4929,1474-0508. doi:[10.1017/S096249291500001X](https://doi.org/10.1017/S096249291500001X).
- [15] M. B. Giles and C. Reisinger. Stochastic finite differences and multilevel Monte Carlo for a class of SPDEs in finance. *SIAM J. Financial Math.*, 3(1):572–592, 2012. ISSN 1945-497X. doi:[10.1137/110841916](https://doi.org/10.1137/110841916).
- [16] M. Gubinelli, P. Imkeller, and N. Perkowski. Paracontrolled distributions and singular PDEs. *Forum Math. Pi*, 3:e6, 75, 2015. ISSN 2050-5086. doi:[10.1017/fmp.2015.2](https://doi.org/10.1017/fmp.2015.2).
- [17] M. Hairer. A theory of regularity structures. *Invent. Math.*, 198(2):269–504, 2014. ISSN 0020-9910,1432-1297. doi:[10.1007/s00222-014-0505-4](https://doi.org/10.1007/s00222-014-0505-4).
- [18] A. Khodadadian, M. Parvizi, M. Abbaszadeh, M. Dehghan, and C. Heitzinger. A multilevel monte carlo finite element method for the stochastic cahn–hilliard–cook equation. *Computational Mechanics*, 64:937–949, 2019. doi:[10.1007/s00466-019-01688-1](https://doi.org/10.1007/s00466-019-01688-1).
- [19] V. Konarovskyi, T. Lehmann, and M.-K. von Renesse. Dean–Kawasaki dynamics: ill-posedness vs. triviality. *Electron. Commun. Probab.*, 24:Paper No. 8, 2019. doi:[10.1214/19-ECP208](https://doi.org/10.1214/19-ECP208).
- [20] V. Konarovskyi, T. Lehmann, and M.-K. von Renesse. On Dean–Kawasaki dynamics with smooth drift potential. *J. Stat. Phys.*, 178:666–681, 2020. doi:[10.1007/s10955-019-02449-3](https://doi.org/10.1007/s10955-019-02449-3).
- [21] L. D. Landau and E. M. Lifshitz. *Course of theoretical physics. Vol. 6*. Pergamon Press, Oxford, second edition, 1987. ISBN 0-08-033933-6; 0-08-033932-8. Fluid mechanics.
- [22] C. McDiarmid. Concentration, probabilistic methods for algorithmic discrete mathematics, 195–248. *Algorithms Combin*, 16, 1998.
- [23] K. W. Morton and D. F. Mayers. *Numerical solution of partial differential equations: an introduction*. Cambridge university press, 2005.
- [24] H. Spohn. *Large scale dynamics of interacting particles*. Springer Science & Business Media, 2012.
- [25] M. te Vrugt, H. Löwen, and R. Wittkowski. Classical dynamical density functional theory: from fundamentals to applications. *Advances in Physics*, 69(2):121–247, 2020. doi:[10.1080/00018732.2020.1854965](https://doi.org/10.1080/00018732.2020.1854965).